Comments on Inorganic Chemistry
Publication details, including instructions for authors and subscription information:
http://www.informaworld.com/smpp/title~content=t713455155

Magnetic Exchange Across the Cyanide Bridge

Høgni Weihe[ab]; Hans U. Güdel[ab]
[a] Institute of Chemistry University of Copenhagen, Copenhagen, Denmark [b] Department of Chemistry and Biochemistry, University of Berne, Bern, Switzerland

To cite this Article Weihe, Høgni and Güdel, Hans U.(2000) 'Magnetic Exchange Across the Cyanide Bridge', Comments on Inorganic Chemistry, 22: 1, 75 — 103
To link to this Article: DOI: 10.1080/02603590008050864
URL: http://dx.doi.org/10.1080/02603590008050864

Magnetic Exchange Across the Cyanide Bridge

HØGNI WEIHE[a*] and HANS U. GÜDEL[b]

[a]*Institute of Chemistry University of Copenhagen, DK-2100 Copenhagen, Denmark and*

[b]*Department of Chemistry and Biochemistry University of Berne CH-3000 Bern, Switzerland*

(Received December 07, 1999)

The superexchange interaction in cyano-bridged transition metal dimers is analysed by a valence bond configuration interaction model in combination with fourth order perturbation theory. Ferro- and antiferromagnetic contributions to the exchange splitting are expressed in terms of metal-ligand hybridization matrix elements, metal-to-ligand, ligand-to-metal, metal-to-metal charge transfer energies, and intra-atomic exhange integrals. The formalism is simplified and we arrive at a two-parameter model, with which it is possible to estimate magnetic ordering temperatures of cubic stoichiometric Prussian Blue like phases containing first row transition metals. The relevance and applicability of our theoretical results is demonstrated on critical temperatures reported in the literature. The model accounts for both ferri- and ferromagnetic ordering temperatures. It is found that cyanide is an efficient mediator of exchange due to the participation of the π and π^* orbitals to equal extent.

Keywords: *cyano bridge; molecular magnetic materials; Preussian Blue analogs; magnetic exchange; exchange interaction; magneto-structural correlation; semi-empirical modeling of critical temperatures*

* Corresponding Author.

Comments Inorg. Chem.
2000, Vol. 22, No. 1-2, pp. 75-103
Reprints available directly from the publisher
Photocopying permitted by license only

1 INTRODUCTION

This Comment has been inspired by recent work on the magnetic properties of Prussian Blue like materials [1]-[10].

It has long been known that Prussian Blue (PB) itself orders ferromagnetically, but at the rather low temperature of 8 K [11]. In 1982 Griebler and Babel reported the first PB like material, namely $CsMn[Cr(CN)_6]$, with an ordering temperature higher than that of liquid nitrogen [12]. This material orders ferrimagnetically at 90 K.

Since then a lot of effort has been put into increasing the ordering temperatures of PB like materials. An immediate expression of the growing amount of literature on this subject is, that the critical temperatures (T_c) are steadily increasing. The state of the art is a T_c of 365 K obtained with a ferrimagnetic material containing hexacyano-chromate(III) anions as well as vanadium(II) cations [2].

The nearest-neighbour transition metal ions in these PB like materials are bridged by cyanide ions. Hence, the shortest metal-metal distance in the cubic lattices is approximately 5.3 Å[1, 10, 13, 14]. With such a large metal-metal distance it is reasonable to neglect direct metal-metal interactions, and a superexchange mechanism[15], i.e. an interaction through the bridging ligand, must be operative. Several models have been proposed to account for the nature of the ordering phenomena. These proposals have been based on the symmetry of the orbitals containing the unpaired metal electrons [5, 6, 16]. Cyanide has several orbitals through which an interaction can be mediated. Babel[6] noticed that an interaction through the cyanide σ orbitals could not explain the experimental evidence available in 1986, whereas an interaction through the π orbitals on cyanide could. Recently, Entley and Girolami[5] argued that mainly the cyanide π^* antibonding orbitals were responsible for the exchange interaction.

All proposals seem to be correct for qualitatively predicting whether the compounds will exhibit ferri- or ferromagnetic ordering. But they are not able to provide any reasonable guesses about the strength of the interaction and the critical temperatures. The aim of this Comment is to add a quantitative element to this subject.

Rather than directly looking at compounds exhibiting spontaneous magnetization below a critical temperature, we begin on a simpler, but for a chemist more natural, level. In Table I we have collected some polynuclear complexes (**1**, **2** and **3**) in which the metal ions are bridged

by cyanide ions. The magnetic properties of these complexes are given in terms of J values across the cyanide bridge in the second column of Table I. J is the parameter in the spin Hamiltonian

$$\hat{H} = J\mathbf{S}_A \cdot \mathbf{S}_B \qquad (1)$$

where $\mathbf{S}_A$ and $\mathbf{S}_B$ are the ground state spin operators of the interacting nearest-neighbour A and B, respectively. In the formulation eqn(1), antiferromagnetic and ferromagnetic splittings are represented with positive and negative J values, respectively. The operator eqn(1) is directly applicable to ions with orbitally non-degenerate ground states. This is the case for all the metal ions mentioned in Table I.

TABLE I Magnetic properties of cyano-bridged transition metal complexes

#	*complex ion*[a]	J_{exp}/cm^{-1}	J_{calc}/cm^{-1}	*ref*
1	$\{Cr[(CN)Mn(trispicmeen)]_6\}^{9+}$	8	16	[17]
2	$\{Cr[(CN)Ni(tetren)]_6\}^{9+}$	−16	−16	[18]
3	$[(NH_3)_5Cr(CN)Cr(NH_3)_5]^{5+}$	32	27	[19]

a. Abbreviations used for terminal ligands are: trispicmeen = N,N,N′-(tris(2- pyridylmethyl)-N′-methyl-ethane)-1,2-diamine, and tetren = tetraethylene- pentaamine.

Considering the large metal-metal separation in cyano bridged complexes, the absolute values of J quoted in Table I are rather high. By a comparison with similar complexes containing hydroxo[20, 21] rather than cyano bridges[17, 18, 19] we conclude that J values for μ-cyano and μ-hydroxo bridged complexes are similar in magnitude. This is at first sight remarkable, since the metal-metal distance in μ-hydroxo bridged complexes is significantly shorter, approximately 3.6–3.7 Å. The first objective of this Comment is to give a reasonable explanation for the relatively large J values obtained for cyano bridged species. The second objective is to explain the signs and magnitudes of the J values in Table I.

Next we will move to extended lattices. In Table II we have collected representative examples of stoichiometric compounds (**4–12**) which exhibit magnetic ordering below a critical temperature T_c, given in the second column. From the mean field theory of ferrimagnetism it can be shown that T_c and the nearest-neighbour J value in the cubic PB like

compounds with the stoichiometry $Q_xB[A(CN)_6]_y$, with Q being a unipositive cation, are approximately related in the following way[1]

$$T_c \approx \frac{y\sqrt{y}}{2k}|J|\sqrt{n_A(n_A+2)n_B(n_B+2)} \qquad (2)$$

where $k = 0.695\ cm^{-1}/K$ is Boltzmann's constant and n_A and n_B are the number of unpaired electrons on metal centers A and B, respectively. Eqn(2) also applies for ferromagnetical materials. In both cases interactions between next-nearest neighbours are neglected. All the compounds **4–12** of Table II have orbitally non-degenerate ground states. Therefore it is meaningful to use eqn(2) to compute a nearest-neighbour J_{exp} value. These are given in the third column of Table II. The third objective of this Comment is to account for the signs and magnitudes of the J_{exp} values of the compounds **4–12**.

TABLE II Critical temperatures and J values of some cubic PB like compounds with the simple $Q_xB[A(CN)_6]_y$ stoichiometry

#[a]	$Q_xB[A(CN)_6]_y$	$\frac{T_c}{K}$	$\frac{J_{exp}}{cm^{-1}}$ [b]	$\frac{J_{calc}}{cm^{-1}}$	$\frac{T_{c,calc}}{K}$ [c]	ref
4	$(V^{IV}O)[Cr^{III}(CN)_6]_{2/3}\cdot\frac{10}{3}H_2O$	115	44	38	101	[1]
5	$KV^{II}[Cr(CN)_6]\cdot 2H_2O$	365	34	29	315	[2]
6	$V^{II}[Cr(CN)_6]_{2/3}\cdot 3.5H_2O$	320	54	29	171	[2]
7*	$CsNi^{II}[Cr^{III}(CN)_6]\cdot 2H_2O$	90	−11.4	−11	86	[3]
8*	$Ni^{II}[Cr^{III}(CN)_6]_{2/3}\cdot 4H_2O$	60	−14	−11	47	[3]
9	$Cr^{II}[Cr^{III}(CN)_6]_{2/3}\cdot\frac{10}{3}H_2O$	240	32	22	162	[4]
10	$Cs_2Mn^{II}[V^{II}(CN)_6]$	125	7.5	17	280	[5]
11	$CsMn^{II}[Cr^{III}(CN)_6]\cdot H_2O$	90	5.5	17	280	[6]
12	$Mn^{II}[Mn^{IV}(CN)_6]\cdot 1.14H_2O$	49	3.0	17	280	[7]

a. The compounds exhibiting ferromagnetic ordering are marked with an asterix. The other ones exhibit ferrimagnetic ordering.
b. The J_{exp} values are extracted from the critical temperatures T_c by use of eqn(2).
c. $T_{c,calc}$ is calculated from eqs(20)-(22) with Q=8.2 cm^{-1}, see section 4.

TABLE III Other PB analogs and their magnetic ordering temperatures

#[a]	*compound*	T_c/K	*ref*
13*	$Ni[Fe(CN)_6]_{2/3}\cdot xH_2O$	23	[8]
14*	$Cu[Fe(CN)_6]_{2/3}\cdot xH_2O$	20	[8]
15	$Co[Fe(CN)_6]_{2/3}\cdot xH_2O$	14	[8]
16	$Mn[Fe(CN)_6]_{2/3}\cdot xH_2O$	9	[8]
17	$Cs_{0.75}[Cr_{2.125}(CN)_6]\cdot 5H_2O$	190	[4]
18	$V^{II}_{0.45}V^{III}_{0.53}[V^{IV}O]_{0.02}[Cr^{III}(CN)_6]_{0.69}(SO_4)_{0.23}\cdot 3H_2O\cdot 0.02K_2SO_4$	310	[9]
19	$Cs_{0.82}V^{II}_{0.66}[V^{IV}O]_{0.34}[Cr^{III}(CN)_6]_{0.92}(SO_4)_{0.203}\cdot 3.6H_2O$	315	[9]
20	$V^{II}_{0.42}V^{III}_{0.58}[Cr(CN)_6]_{0.86}\cdot 2.8H_2O$	315	[10]

a. The compounds exhibiting ferromagnetic ordering are marked with an asterix. The other ones exhibit ferrimagnetic ordering.

In Table III we have collected some additional PB type compounds (**13–20**) which also exhibit ordering phenomena. They either contain ions with orbitally degenerate groundstates (**13–16**), or contain metal ions with both high-spin and low-spin groundstates (Cr^{II} in **17**), or have rather complicated stoichiometries (**18–20**). Therefore, the formalism in eqs(1) and (2) is not really meaningful for these substances. However, they are certainly interesting and they will be included when we come to the fourth and final objective of this comment, which is a discussion and comparison of the T_c's of **4–20**, Table II and III.

With these four objectives in view we introduce in the next section a valence bond configuration interaction (VBCI) model[22] which will be the framework of our calculations and discussion.

2 A VALENCE BOND CONFIGURATION INTERACTION MODEL FOR A-CN-B

In this section we adapt the VBCI model[22] to the PB like materials in which a cyanide ion is a linear bridge between two metal ions *A* and *B*. We assume that the metal ions interact via the bonding π and the anti-bonding π^* orbitals on the cyanide ion. The present treatment has some analogies to our earlier treatment of the *A-L-B* system[23], in which the bridging ligand *L* has only one orbital. But the fact that cyanide has two available orbitals makes the cyano bridging ligand slightly different from a mono-atomic bridging ligand. The interacting orbitals in the xz plane and, by analogy, in the yz plane are shown in Figure 1. The hybridization matrix elements describing the one-electron interaction between *A*and cyanide and between cyanide and *B* are in the following designated as follows:

$$V_a = \langle a|\hat{h}|\pi\rangle = \langle \pi|\hat{h}|a\rangle \tag{3}$$

$$V_b = \langle b|\hat{h}|\pi\rangle = \langle \pi|\hat{h}|b\rangle \tag{4}$$

$$V_a^* = \langle a|\hat{h}|\pi^*\rangle = \langle \pi^*|\hat{h}|a\rangle \tag{5}$$

$$V_b^* = \langle b|\hat{h}|\pi^*\rangle = \langle \pi^*|\hat{h}|b\rangle \tag{6}$$

where $\hat{h}$ is the one-electron part of the Hamiltonian. At this point it is important to recall the usual approximation [24] that such one-electron

matrix elements are proportional to the overlap integrals between the interacting orbitals. Referring to Figure 1, one of the relevant overlaps, namely $\langle \pi_x | b \rangle$, has the opposite sign of the three others. Hence, V_b has the opposite sign of V_a, V_a^* and V_b^*.

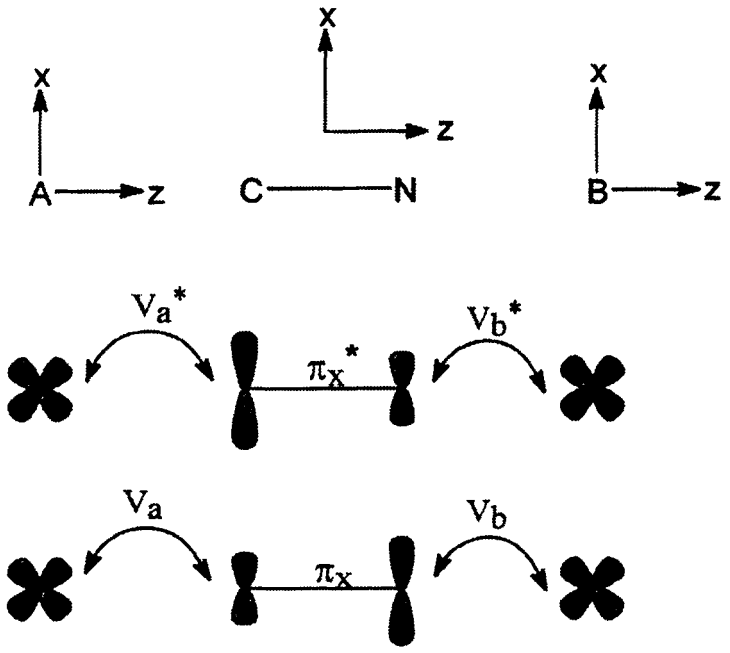

FIGURE 1 Interacting orbitals with π symmetry in the A-CN-B bridging arrangement

The present VBCI treatment will be slightly simpler than the one in ref.[23]. The method is outlined in [23] and will not be repeated here. In essence, the exchange splitting in the ground electron configuration is obtained by interaction of the ground electron configuration with various excited configurations. Besides the ground electron configuration, we only include ligand to metal electron transfer (LMCT), metal to ligand electron transfer (MLCT) and metal to metal electron transfer (MMCT) electron configurations in which *one* electron has been transferred.

All functions from each configuration are generated as described in ref[23], and then the key matrix elements

$$\langle S'\Gamma' M'_S M'_\Gamma | \hat{h} | S\Gamma M_S M_\Gamma \rangle \tag{7}$$

are calculated. The eigenvalues of the matrices thus obtained will be examined with non-degenerate perturbation theory up to fourth order [25]. In the following three sections we treat the three cases where

i) *a* is half-filled and *b* is half-filled

ii) *a* is half-filled and *b* is empty or vice versa

iii) *a* is half-filled and *b* is full or vice versa

The final possibility, namely the case where *a* is full and *b*is empty will not be treated here, because the contribution from this interaction to the net *J* is small[23].

2.1 $J_i^{\pi\pi^*}$: *a* half filled and *b* half-filled

The relevant electron configurations with their zero-order energies are illustrated in Figure 2. The ground electron configuration I, LMCT configurations II and III, as well as the MLCT configurations VI and VII all give rise to spin singlets (S=0) and spin triplets (S=1), whereas the MMCT configurations IV and V give rise to singlets only. Since we do not take into account two-center two-electron exchange integrals, the singlet and triplet of the ground configuration I are degenerate in the absence of CI. The same applies for configurations II, III, VI and VII.

The CI matrices for the singlet and triplet spin multiplets of this particular four electron system with n_A=n_B=1 are given in appendix A. For n_A and n_B unpaired electrons on centers *A* and *B*, respectively, the expression for the contribution to *J* is found to be

$$J_i^{\pi\pi^*} = \frac{1}{n_A n_B}\left\{ V_a^2 V_b^2 \left[\frac{2}{\Delta_B^2 U_{AB}} + \frac{2}{\Delta_A^2 U_{BA}}\right] + V_a^{*2} V_b^{*2}\left[\frac{2}{\Delta_B^{*2} U_{BA}} + \frac{2}{\Delta_A^{*2} U_{AB}}\right] - V_a V_b V_a^* V_b^*\left[\frac{4}{U_{AB}\Delta_B\Delta_A^*} + \frac{4}{U_{BA}\Delta_A\Delta_B^*}\right]\right\} \tag{8}$$

which is correct to fourth order in perturbation theory. The first two terms have a conventional form which is also found in systems with

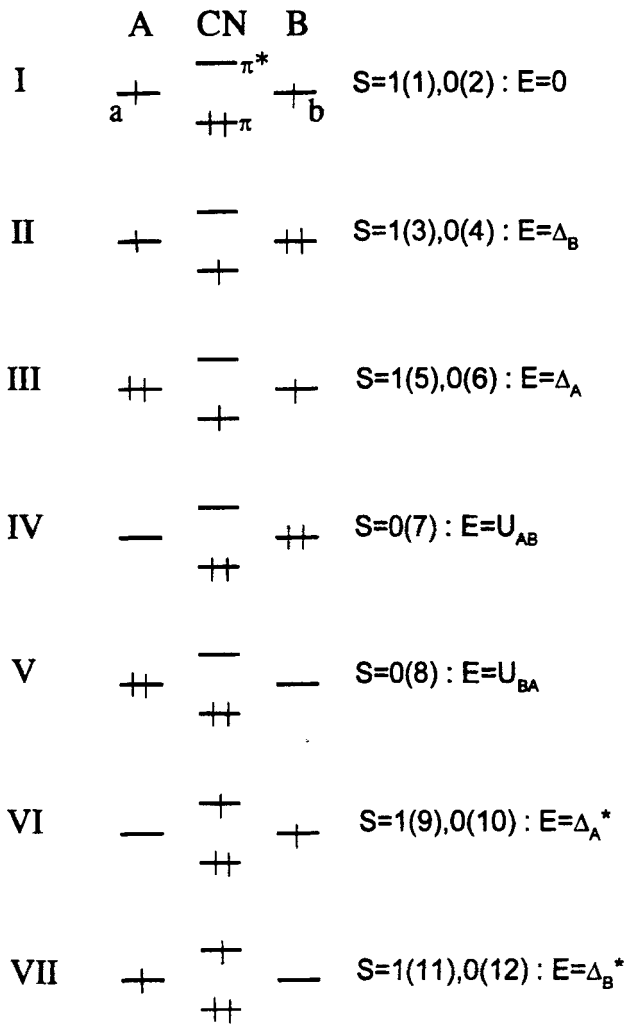

FIGURE 2 Illustrations of the configurations included in the VBCI model for the case when the cyanide π and π^* orbitals interact with half-filled orbitals on metal centers *A* and *B* (section 2.1). Configuration I represents the ground electron configuration, II and III represent ligand LMCT electron configurations, IV and V represent MMCT electron configurations, and finally VI and V represent MLCT electron configurations. Possible spin values and zero-order energies are given to the right of each configuration. The numbers in parentheses refer to basis function numbers used in Appendix A

mono-atomic bridges. The first term describes the interaction between a and b through the π bonding ligand orbital, and the second term describes the interaction through the π^* antibonding ligand orbital. Since the electron configuration $a^1\pi^{*0}b^1$ is the hole-electron equivalent of the configuration $a^1\pi^2b^1$, the first two terms have the same form. The third term is new, it is a cross term which results from the simultanious presence of the two ligand orbitals π and π^*. Since V_b is negative while V_a, V_a^* and V_b^* all are positive, the three terms of eqn(8) all contribute to $J_i^{\pi\pi^*}$ with the same sign, namely positively, *i.e.* antiferromagnetically.

2.2 $J_{ii}^{\pi\pi^*}$: a half filled and b empty

The four relevant electron configurations with their zero-order energies are illustrated in Figure 3. The configurations I, II, III and IV represent the ground, LMCT, MMCT and MLCT electron configurations, respectively. The situation here is slightly more complicated than in the previous section, since we now have the possibility to generate excited configurations with two unpaired electrons on center B, see configurations II and III in Figure 3. According to Hund's rule, the triplet of the sub configuration $b_1^1b_2^1$ is lower in energy than the corresponding singlet by the quantity $\mathcal{I}_2$, which is a measure of one-center two-electron exchange integrals as discussed in section 3. [23, 30].

The configuration interaction matrices for this particular four electron system with n_A=n_B=1 are given in appendix B. For n_A and n_B unpaired electrons on centers A and B, respectively, the expression for the contribution to J is found to be

$$J_{ii}^{\pi\pi^*} = \tag{9}$$
$$-\frac{1}{n_A(n_B+1)}\left\{V_a^2V_b^2\left[\frac{2}{\Delta_B^2U_{AB}}-\frac{2}{(\Delta_B+\mathcal{I}_{n_B+1})^2(U_{AB}+\mathcal{I}_{n_B+1})}\right]\right.$$
$$+V_a^{*2}V_b^{*2}\left[\frac{2}{\Delta_A^{*2}U_{AB}}-\frac{2}{\Delta_A^{*2}(U_{AB}+\mathcal{I}_{n_B+1})}\right]$$
$$\left.-V_aV_bV_a^*V_b^*\left[\frac{4}{\Delta_A^*\Delta_BU_{AB}}-\frac{4}{\Delta_A^*(\Delta_B+\mathcal{I}_{n_B+1})(U_{AB}+\mathcal{I}_{n_B+1})}\right]\right\}$$

which is correct to fourth order in perturbation theory. Assuming Δ_B and $\mathcal{I}_{n_B+1} \ll U_{AB}$ [32] this simplifies to

$$J_{ii}^{\pi\pi^*} = -\frac{1}{n_A(n_B+1)}\left[\quad 2\frac{V_a^2V_b^2}{\Delta_B^2U_{AB}}\frac{2U_{AB}+\Delta_B}{U_{AB}}\right.$$
$$+2\frac{V_a^{*2}V_b^{*2}}{\Delta_A^{*2}U_{AB}}$$
$$\left.-4\frac{V_aV_bV_a^*V_b^*}{\Delta_A^*\Delta_BU_{AB}}\frac{U_{AB}+\Delta_B}{\Delta_B}\right]\frac{\mathcal{I}_{n_B+1}}{U_{AB}} \qquad (10)$$

As in section 2.1 eqn(8), the first, second and third terms in the square bracket correspond to the interaction through the π orbital, the interaction through the π^* orbital and to the cross term, respectively. The electron configurations relevant for the interaction through the π and π^* orbital are $a^1\pi^2b^0$ and $a^1\pi^{*0}b^0$, respectively. These electron configurations are not hole-electron equivalents of each other and therefore the first two terms do not have the same form. All three terms in eqn(10) contribute to $J_{ii}^{\pi\pi^*}$ with the same sign, resulting in $J_{ii}^{\pi\pi^*}$ being negative. Finally, notice that this contribution to net J is proportional to $1/n_A(n_B+1)$ [23, 30], and not to $1/n_An_B$ as reported in the older literature [29].

2.3 $J_{iii}^{\pi\pi^*}$: *a* half filled and *b* full

The relevant electron configurations and their zero-order energies are given in Figure 4. The configuration interaction matrices for this particular system with n_A=n_B=1 are given in appendix C. For n_A and n_B unpaired electrons on centers A and B, respectively, the expression for the contribution to J is found to be

$$J_{iii}^{\pi\pi^*} = \qquad (11)$$
$$-\frac{1}{n_A(n_B+1)}\left\{V_a^2V_b^2\left[\frac{2}{\Delta_A^2U_{BA}}-\frac{2}{\Delta_A^2(U_{BA}+\mathcal{I}_{n_B+1})}\right]\right.$$
$$+V_a^{*2}V_b^{*2}\left[\frac{2}{\Delta_B^{*2}U_{BA}}-\frac{2}{(\Delta_B^{*2}+\mathcal{I}_{n_B+1})^2(U_{BA}+\mathcal{I}_{n_B+1})}\right]$$
$$\left.-V_aV_bV_a^*V_b^*\left[\frac{4}{\Delta_A\Delta_B^*U_{BA}}-\frac{4}{\Delta_A(\Delta_B^*+\mathcal{I}_{n_B+1})(U_{BA}+\mathcal{I}_{n_B+1})}\right]\right\}$$

which is correct to fourth order in perturbation theory. Assuming Δ_B^* and $\mathcal{I}_{n_B+1} \ll U_{BA}$ [32] this simplifies to

$$J_{iii}^{\pi\pi^*} = -\frac{1}{n_A(n_B+1)}\left[\ 2\frac{V_a^2V_b^2}{\Delta_A^2U_{BA}}\right.$$
$$+2\frac{V_a^{*2}V_b^{*2}}{\Delta_B^{*2}U_{BA}}\frac{2U_{BA}+\Delta_B^*}{U_{BA}}$$
$$\left.-4\,\frac{V_aV_bV_a^*V_b^*}{\Delta_A\Delta_B^*U_{BA}}\frac{U+\Delta_B^*}{\Delta_B^*}\ \right]\frac{\mathcal{I}_{n_B+1}}{U_{BA}} \qquad (12)$$

As in the previous two sections we note that the first, second and third term in the square bracket correspond to the interactions through the π orbital, the π^* orbital and to the cross term, respectively. Notice that the form of the first and second terms corresponds to the second and first terms in eqn(10), respectively, whereas the third term has the same form in both eqs(10) and (12). They all contribute with the same sign, resulting in $J_{iii}^{\pi\pi^*}$ being negative.

3 MODEL PARAMETERS

Before applying the above formalism to the real systems, a brief discussion of the various model parameters and also their relative magnitudes is in order. In hexacyano complexes with di- and trivalent 3d transition metal ions, LMCT transitions involving π ligand and t_{2g} metal 3d orbitals have been reported at energies ranging from 30000 cm^{-1} to 37200 cm^{-1}[26]. In the same type of complexes, MLCT transitions involving t_{2g} metal and π^* ligand orbitals have been reported at energies ranging from 41000 cm^{-1} to 50000 cm^{-1}[26]. Hence, all the LMCT and MLCT energies appearing in the model are comparable in magnitude, and we make the approximation $\Delta_A = \Delta_B = \Delta_A^* = \Delta_B^* = \Delta$.

The ratios VV'/Δ, with $V,V'=V_a$, V_a^*, V_b or V_b^* and and $\Delta=\Delta_A$, Δ_A^*, Δ_B or Δ_B^*, are related to and have the order of magnitude of of ligand field parameters [23]. Therefore, it is important to briefly discuss the π donor and the π^*acceptor properties of both the carbon and the nitrogen end of the cyanide bridging ligand. They are both situated at the high end of ligand-field strengths in the spectrochemical series, and in a first approximation we assume that they have the same total strength. From the fact that in the optical spectra of the complexes $[Cr(NH_3)_5CN]^{2+}$[27] and $[(NH_3)_5CrCNCr(NH_3)_5]^{5+}$[19] the first two spin-allowed ligand-field bands are not split, we conclude that the π

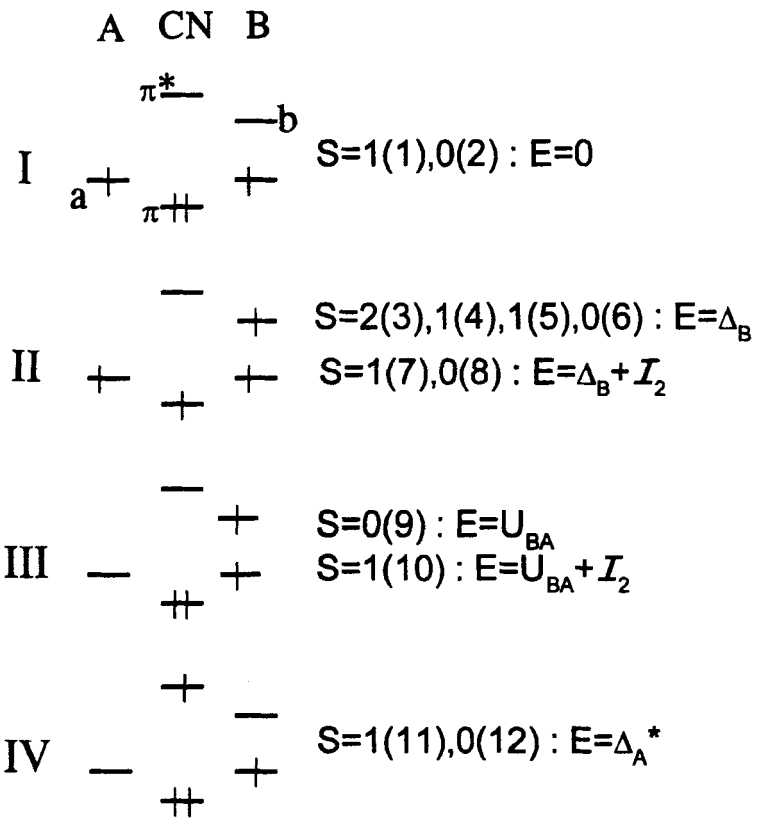

FIGURE 3 Illustrations of the configurations in the VBCI model for the case when the cyanide π and π^* orbitals interact with a half-filled orbital *a* on center *A* and an empty orbital *b* on center *B* (section 2.2). Configurations I, II, III and IV represent the ground, a LMCT, a MMCT and a MLCT electron configuration, respectively. Possible spin values and zero-order energies are given to the right of each configuration. The numbers in parentheses refer to basis function numbers used in Appendix B

donor and π acceptor strengths are similar at both ends. In an ab initio study [28] of $[Cr(CN)_6]^{3+}$ it was found that cyanide carbon-coordinated to chromium(III) acts as a π donor and acceptor to equal extents. We therefore make the further assumption that they are the same, and we

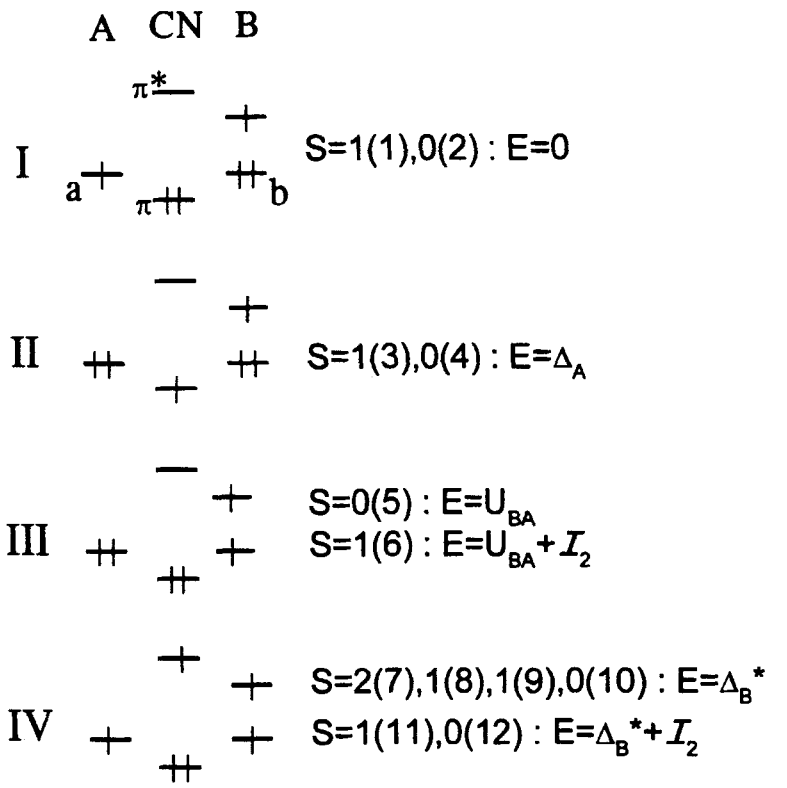

FIGURE 4 Illustrations of the configurations in the VBCI model for the case when the cyanide π and π^* orbitals interact with a half-filled orbital a on metal center A and a full orbital b on metal center B (section 2.3). Configurations I, II, III and IV represent the ground, a LMCT, a MMCT and a MLCT electron configuration, respectively. Possible spin values and zero-order energies are given to the right of each configuration. The numbers in parentheses refer to basis function numbers used in Appendix C

have for the hybridisation matrix elements in eqs(3)-(6): $V_a = V_a^* = V_b = V_b^* = V$.

For compounds in which the metals A and B are in the same oxidation state, upper limits of the MMCT energies U_{AB} and U_{BA} can in principle be estimated from the free-ion ionization potentials. For di- and tri-valent transition metal ions the U values thus obtained are in the

interval 14 – 24eV. However, these values are drastically reduced in a solid due to covalency effects. For isovalent A and B ions, reasonable U values entering models as the one presented here are of the order 5–10eV (≈40000–80000 cm^{-1})[22]. For compounds in which A and B are different metals and have different oxidation states, the U values cannot be simply estimated from the free-ion ionization potentials. In general U values are reduced, and in so-called mixed-valence compounds, in which A and B represent the same ion in different oxidation states, the first allowed absorption band in the optical spectrum is due to an intervalence transition and thus is mainly of MMCT character. Prussian Blue itself is a notable example for this class of compounds, with an intense broad absorption centered around 15000 cm^{-1} leading to the deep blue colour. None of the compounds in Tables II and III has been reported to exhibit a low-lying intervalence absorption, and we therefore assume that the first allowed intercenter electronic excitation is of LMCT or MLCT character. For our calculations we therefore assume, as we did in ref[23], that the following relation holds: $\frac{1}{2}U < \Delta < U$.

Equations (10) and (12) which both contribute ferromagnetically to the net J value both contain the factor $\mathcal{I}_{n_B+1}/U$. $\mathcal{I}_{n_B+1}$ can be expressed as follows[30]

$$\mathcal{I}_{n_B+1} = (n_B + 1)I \tag{13}$$

where I is an average one-center-two-electron exchange integral; $I = C + \frac{5}{2}B$ with B and C being the Racah repulsion parameters. I is of the order 4000–5000 cm^{-1}[30]. In a recent analysis [31] of the magnetic properties of several oxo bridged dimers of trivalent transition metal ions we used the ratio I/U as an effective parameter and a value of $I/U \approx 0.25$ was obtained in the analysis[23]. This rather high value is mainly a result of the very restricted model. If the model is extended to also include hybridizations with higher-lying electron configurations such as double LMCT, then it is possible to get I/U ratios of the order 0.1, which appear more reasonable [23].

As a result of all the approximations discussed above we can now reduce the formalism to the following tractable and very simple form with only two parameters

$$J_i^{\pi\pi^*} = \frac{16}{n_A n_B} \mathcal{Q} \tag{14}$$

$$J_{ii}^{\pi\pi^*} = J_{iii}^{\pi\pi^*} = -\frac{2}{n_A} \mathcal{Q}\mathcal{W} \tag{15}$$

where $\mathcal{Q}$ is defined as

$$\mathcal{Q} = \frac{V^4}{\Delta^2 U} \tag{16}$$

and $\mathcal{W}$ is defined as

$$\mathcal{W} = \left[1 + \frac{2U + \Delta}{U} + 2\frac{U + \Delta}{\Delta}\right] \frac{I}{U} \tag{17}$$

From the prefactors of eqs(14) and (15) we see that if both terms $J_i^{\pi\pi^*}$ and $J_{ii}^{\pi\pi^*} = J_{iii}^{\pi\pi^*}$ contribute to the net J, then the former will dominate. For A and B being both transition metals the prefactors of eqs(14) and (15) can vary between the limits $16 \geq \frac{16}{n_A n_B} \geq \frac{16}{25}$ and $2 \geq \frac{2}{n_A} \geq \frac{2}{5}$, respectively.

The value of the dimension-less parameter $\mathcal{W}$ is strongly restricted by the model and to some extent by our approximations. With $\frac{1}{2}U < \Delta < U$ and $0.1 < I/U < 0.25$ we expect $\mathcal{W}$ to be close to unity, i.e.

$$\mathcal{W} \approx 1 \tag{18}$$

The parameters $\mathcal{Q}$ and $\mathcal{W}$ will be adjusted to fit the experimental J values.

4 CALCULATION OF J

By an example we now illustrate how eqs(14) and (15) are used to obtain expressions for the relevant ground state J_{calc} values for the electron configurations represented by the compounds listed in Tables I and II. Let A and B be Cr^{3+} and VO^{2+}, respectively, corresponding to **4** from Table II. The geometry of the dimeric Cr-CN-VO unit is shown in

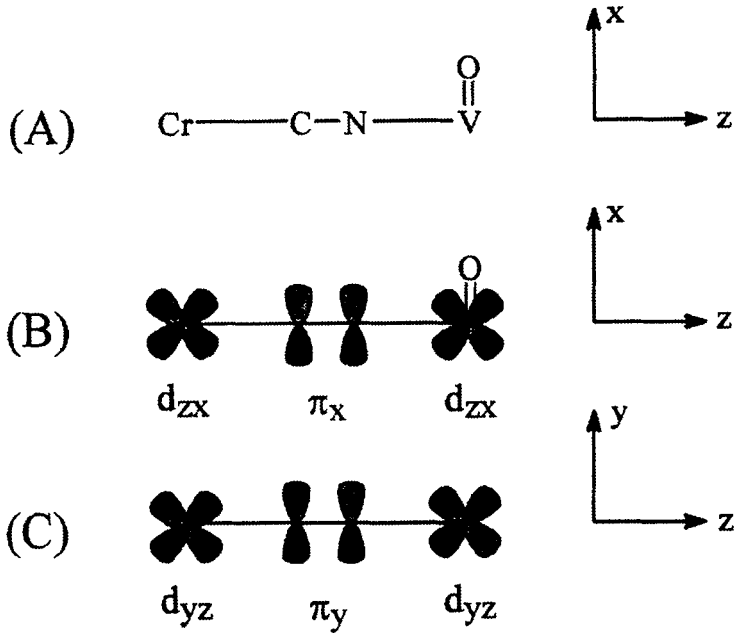

FIGURE 5 Definition of coordinate system for the chromium-cyanide-vanadyl structural unit (A), and illustration of the orbitals involved in the ferromagnetic (B) and antiferromagnetic (C) contributions to net *J*. See section 4 for details

Figure 5. With the coordinate system defined in Figure 5, the ground electron configuration of the Cr-CN-VO unit is $(d^1_{xy}d^1_{yz}d^1_{zx})_{Cr}(\pi^2)_{CN}(d^1_{zx})_{VO}$. The π_x, π^*_x ligand orbitals interact with the d_{zx} metal orbitals, while the π_y, π^*_y ligand orbitals interact with the d_{yz} metal orbitals. The J_{calc} expression for this unit is composed of two terms, namely an antiferromagnetic (positive) term $J_i^{\pi\pi^*}$ since the $(d_{zx})_{Cr}$ and $(d_{zx})_{VO}$ are both half-filled, and a ferromagnetic (negative) term $J_{ii}^{\pi\pi^*}$ since the $(d_{yz})_{Cr}$ and $(d_{yz})_{VO}$ are half-filled and empty, respectively. The d_{xy} metal orbitals do not interact, since they have δ symmetry with respect to the Cr-CN-V axis. Application of

eqs(14) and (15) results in the following expression for J_{calc} relevant for the Cr-CN-VO unit

$$J_{calc} = \frac{16}{n_{Cr}n_{VO}}\mathcal{Q} - \frac{2}{n_{Cr}}\mathcal{Q}\mathcal{W} = \frac{16}{3}\mathcal{Q} - \frac{2}{3}\mathcal{Q}\mathcal{W} \qquad (19)$$

By using this procedure for the other electron configurations represented by the compounds in Tables I and II, we obtain all the relevant J_{calc} values. They are collected in Table IV. The factor of 2 appearing in most of the expressions in Table IV is due our assumption that the interactions through the π_x, π_x^* and π_y, π_y^* orbitals of cyanide by assumption contribute equally to the net J value.

TABLE IV Theoretical expressions for J_{calc} in terms of the parameters $\mathcal{Q}$ and $\mathcal{W}$ defined in eqs(16) and (17), respectively

(A,B)	J_{calc}
$(Mn^{2+},Cr^{3+}),(Mn^{2+},V^{2+}),(Mn^{2+},Mn^{4+})$	$2\frac{16}{15}\mathcal{Q}$
(Ni^{2+},Cr^{3+})	$-2\frac{2}{3}\mathcal{Q}\mathcal{W}$
$(Cr^{3+},Cr^{3+}),(V^{2+},Cr^{3+})$	$2\frac{16}{9}\mathcal{Q}$
(Cr^{3+},VO^{2+})	$\frac{16}{3}\mathcal{U} - \frac{2}{3}\mathcal{Q}\mathcal{W}$
(Cr^{2+},Cr^{3+})	$2\frac{16}{12}\mathcal{U}$

We will now apply the formalism developed above to the model compounds of Table I. In the rest of this Comment we assume that the two effective parameters $\mathcal{Q}$ and $\mathcal{W}$ are transferable between dimers irrespective of the oxidation states of the constituent metal ions.

The expressions for J_{calc} in Table IV are fitted to the J_{exp} values in Table I, with $\mathcal{Q}$ and $\mathcal{W}$ as adjustable parameters. The least-squares fit yields the parameter values $(\mathcal{Q},\mathcal{W}) = (7.6\ \mathrm{cm}^{-1}, 1.6)$. The $\mathcal{Q}$ value

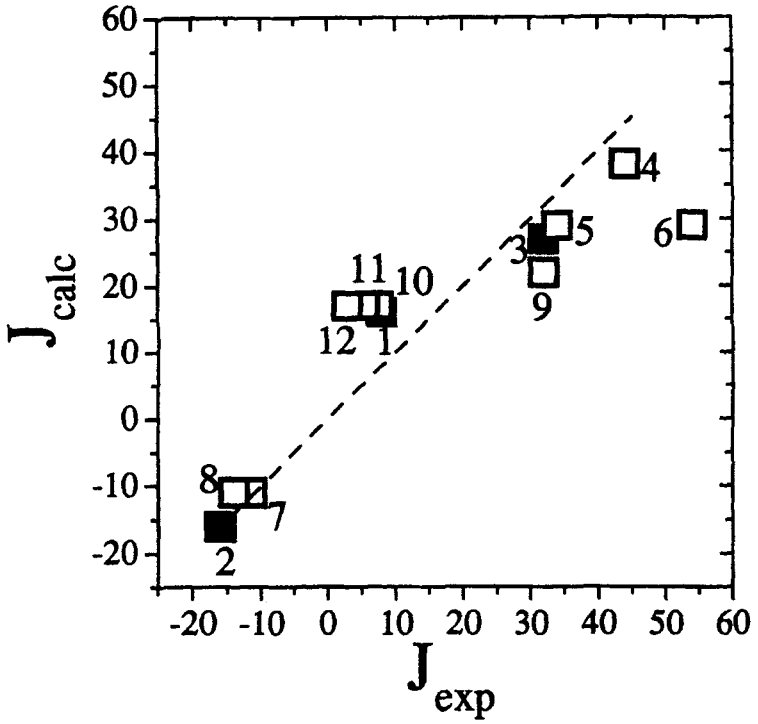

FIGURE 6 Correlation of J_{calc} and J_{exp}values. Filled and open squares correspond to the data from Table I and II, respectively

represents a reasonable average, since if **1** and **3** are analysed separately and independently with the relevant expressions from Table IV and the J_{exp} values from Table I, $\mathcal{Q}$ values of 4 and 9 cm^{-1}, respectively, are obtained. The value of $\mathcal{W}$ also has the expected magnitude, see eqs(17) and (18). The calculated J_{calc} values using the obtained parameter values are given in the fourth column of Table I, and graphically represented in Figure 6.

Repeating the fitting procedure to the J_{exp} values of the PB analogs in Table II yields the parameter values $(\mathcal{Q}, \mathcal{W}) = (8.2\ cm^{-1}, 1.03)$, in good agreement with the parameter values from the previous paragraph and our expectation (eqn(18)). The J_{calc} values obtained using these

parameters are given in the fifth column of Table II, and graphically represented in Figure 6. We are now in a position to discuss the first three objectives of this Comment.

1: Why is the absolute magnitude of the exchange parameters large despite the large metal-metal separation? All effects of one-center two-electron exchange interactions on the possible inter-center electronic excitations are contained in the parameter $\mathcal{W}$. If the *A*-CN-*B* interaction was mediated solely through either the π or the π^* orbitals of cyanide, then the expression for $\mathcal{W}$ eqn(17) would be reduced to either of the first two terms, recall sections 2.2 and 2.3. Hence, a value of $\mathcal{W}$ of 0.1–0.25 [23] would be expected. The value of $\mathcal{W} \approx 1$ results from the action of all the terms in eqn(17). This validated our assumption that both π and π^* orbitals of cyanide participate with comparable magnitude in the interaction. Recently, this was also assumed valid in a first principle calculation of *J* in cyano-bridged species[33]. There it was concluded that the interaction through the σ orbitals of cyanide was significantly smaller compared to the interaction through the π and π^* orbitals. This is in agreement with the observation of Babel[6].

2,3: Can we account for the sign and magnitude of the observed *J* parameter? The comparison between experimental and calculated *J* values is illustrated in Figure 6. The agreement is remarkably good throughout the series of cluster compounds (Table I) and PB analogs (Table II), considering the numerous approximations we had to introduce. The signs and gross trends are nicely reproduced. The consistency of the parameter values obtained for the two classes of compounds clearly illustrates that studying molecular polynuclear complexes certainly provides useful information about extended lattices.

5 T_C IN PB ANALOGS

Since the critical temperature is related to *J* by eqn(2) we can now directly calculate how T_c depends on the number of unpaired electrons on the interacting metal centers.

We first consider the situation when both π_x, π_x^* and π_y, π_y^* interact with half-filled orbitals on both metal centers. Both interaction pathways ((π_x, π_x^*) and (π_y, π_y^*)) are antiferromagnetic and by combination of eqs (2) and (14) we obtain that for materials in which the

nearest-neighbour interaction is purely antiferromagnetic and which order ferrimagnetically, the critical temperature T_c is given as

$$T_c = \frac{Qy\sqrt{y}}{2k}\left[\frac{32}{n_A n_B}\sqrt{n_A(n_A+2)n_B(n_B+2)}\right] \qquad (20)$$

Since we have the requirement that two unpaired electrons on A are interacting with two unpaired electrons on B, eqn(20) is only valid for $n_A \geq 2$ and $n_B \geq 2$. The critical temperature eqn(20) is plotted in Figure 7 for different combinations of n_A and n_B.

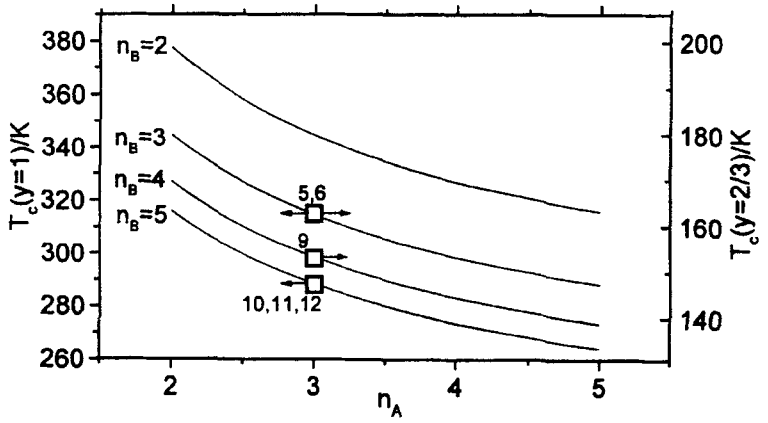

FIGURE 7 Calculated critical temperatures for PB analogs in which two antiferromagnetic exchange pathways contribute to the net J value, eqn(20). y is the A/B ratio in the PB formula. Examples from Table II are indicated

Similarily, by combining eqs (2) and (15) we obtain that for materials in which the nearest-neighbour interaction is ferromagnetic and which order ferromagnetically, the critical temperature is given as

$$T_c = \frac{Qy\sqrt{y}}{2k}\left[\frac{4}{n_A}\sqrt{n_A(n_A+2)n_B(n_B+2)}\right] \qquad (21)$$

where we for simplicity set $\mathcal{W} = 1$. Here we have the requirement that $n_A \geq 2$. The critical temperature eqn(21) is plotted in Figure 8 as a function of n_A and n_B.

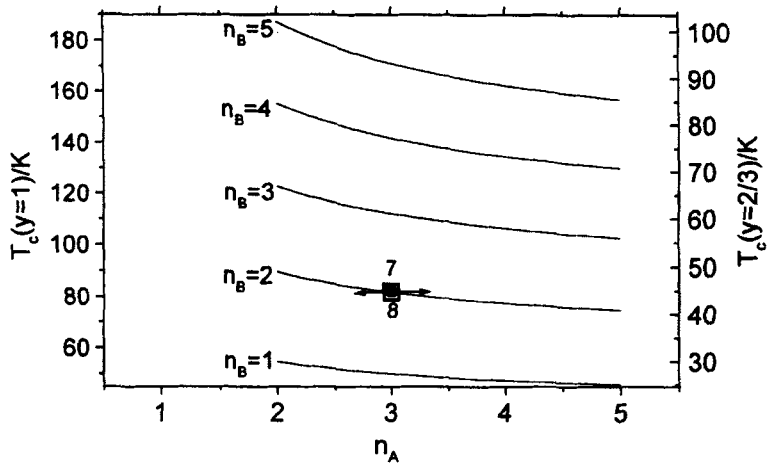

FIGURE 8 Calculated critical temperatures for PB analogs in which two ferromagnetic exchange pathways contribute to the net J value, eqn(21). Examples from Table II are indicated

Finally, when one set of the ligand orbitals, say π_x and π_x^*, contributes negatively to the net J, and the other set, i.e. π_y and π_y^*, contributes positively to net J, then the critical temperature is given as

$$T_c = \frac{\mathcal{Q}y\sqrt{y}}{2k}\left[\frac{(16-2n_B)}{n_A n_B}\sqrt{n_A(n_A+2)n_B(n_B+2)}\right] \qquad (22)$$

where we again set $\mathcal{W} = 1$. This combination requires $n_A \geq 2$. The critical temperature eqn(22) is plotted in Figure 9 as a function of n_A and n_B.

Comparing the ordinate axes of Figures 7–9, we immediately see that the highest critical temperatures are expected for materials in which both interaction pathways contribute antiferromagnetically to the net J (Figure 7 and eqn(20)). For these materials, exemplified by **5,6** and **9–12** from Table II, the critical temperature is expected to lie in the range 240–360 K and 140–240 K for y = 1 and $y = \frac{2}{3}$, respectively.

If there exist two ferromagnetic exchange pathways (**7** and **8** from Table II) between the two interacting metal centers (Figure 8 and

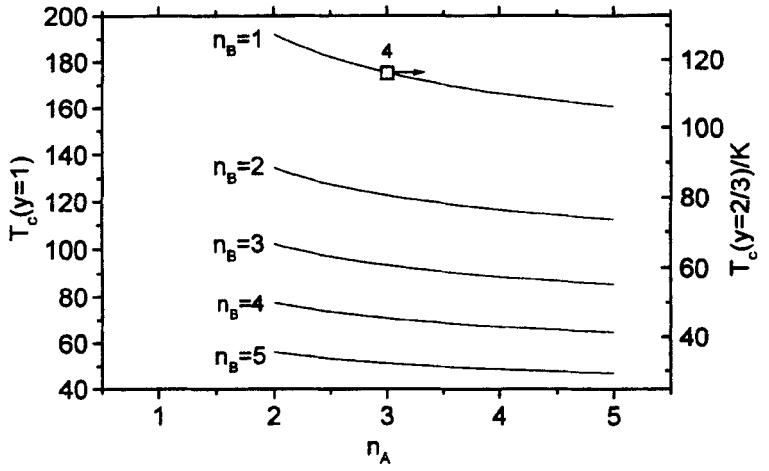

FIGURE 9 Calculated critical temperatures for PB analogs in which one antiferromagnetic and one ferromagnetic pathway contribute to the net J value, eqn(22). Compound **4** from Table II is indicated as an example

eqn(21)) then the critical temperature is expected to lie in the range 50–190 K and 25–100 K for $y = 1$ and $y = \frac{2}{3}$, respectively.

The situation with one antiferromagnetic and one ferromagnetic exchange pathway (Figure 9 and eqn(22)) leads to similar ranges of critical temperatures as discussed for Figure 8. The only example of this situation is compound **4** from Table II.

Notice the qualitative difference between the cases where antiferromagnetic (Figures 7 and 9) and ferromagnetic (Figure 8) contributions to J dominate. In the former case the highest T_c's are obtained for n_A and n_B both as low as possible. In the latter case high T_c's are obtained for small n_A and large n_B values.

The calculated T_c's corresponding to the n_A and n_B values represented by **4–12** are given in the sixth column of Table II, and have been marked in Figures 7–9. The comparison with the experimental critical temperatures shows an overall good agreement. The discrepancies are mainly a result of our assumption of perfect transferability of $\mathcal{Q}$ and $\mathcal{W}$ between all the compounds. For compounds **10, 11** and **12**, the agree-

ment is worst, and the observed decrease of T_c in this series is not reproduced by the model. This can be explained by referring directly to eqn(8). Due to the higher charge of Mn^{4+}compared to V^{2+}, the d orbitals of V^{2+} are more diffuse than those of Mn^{4+}. This implies that the transfer integrals show the following trend: $V_{V^{2+}} > V_{Cr^{3+}} > V_{Mn^{4+}}$ and $V^*_{V^{2+}} > V^*_{Cr^{3+}} > V^*_{Mn^{4+}}$. MLCT energies increase with the oxidation state of the metal, i.e., $\Delta^*_{Mn^{4+}} > \Delta^*_{Cr^{3+}} > \Delta^*_{V^{2+}}$, while the opposite holds for LMCT transitions. Using such refinements of our model we can understand the observed trend in T_c for **10, 11** and **12**, in agreement with ref.[5].

The compounds **13–21** collected in Table III cannot be treated quantitatively with our formalism, since orbital non-degeneracy and a simple $Q_xA[B(CN)_6]_y$ stoichiometry is a necessary requirement for eqn(1) and (2). We can, however, discuss the critical temperatures of the compounds of Table III semiquantitatively based on the number of unpaired electrons.

The ferromagnetic ordering temperatures of compounds **13** and **14** can be directly compared. The number of possible exchange pathways is determined by the electron occupancy of the metal ions. Both ions contain low spin Fe^{3+} with an electron configuration t_2^5. The Ni^{2+} and Cu^{2+} ions have the electron configuration $t_2^6e^2$ and $t_2^6e^1$, , respectively. We thus have a half-filled orbital of Fe^{3+} interacting with a full orbital on Ni^{2+} or Cu^{2+}. This gives a negative contribution (eqn(12)) to the exchange splitting. No positive contributions are possible. Hence, the ferromagnetic ordering is explained. If the n_A, n_B dependence eqn(21) and Figure 8 was applicable we would expect T_c(**13**)>T_c(**14**). This is in agreement with the experimental facts, but the experimental T_c's are very similar.

In a similar way, the critical temperatures of compounds **15** and **16** can be compared. By considering the t_2 electron configurations of the metal ions we conclude that there are both negative and positive contributions to the net J value. If eqn(22) and Figure 9 was applicable we would expect T_c(**15**) (n_A=1,n_B=3) to be higher than T_c(**16**) (n_A=1,n_B=5). This again is in agreement with the experimental facts.

Based on simple stoichiometry arguments one should expect T_c(**17**)> T_c(**9**) since y(**17**)>y(**9**). However, the opposite was found, and the authors of ref[4] showed that part of the Cr^{2+} ions in **17** have the low-spin ground state. The low-spin Cr^{2+} ions have one doubly occupied t_2 orbital which adds a ferromagnetic contribution to the net J

which as a result gets reduced. This, apart from the non-simple stoichiometry, explains part of the unexpected reversal of T_c between **9** and **17**.

It is certainly remarkable that the compounds **5,6,18–20** with the highest ordering temperatures all contain the metal ions Cr^{3+}as well as V^{2+} or V^{3+}. These metal ions have two (V^{3+}) or three (Cr^{3+}, V^{2+}) unpaired electrons in their ground states. Hence, there are two possible antiferromagnetic interaction pathways. According to our model, this combination of n_A and n_B should lead to the highest possible critical temperatures, see Figure 7.

6 CONCLUSION

By adapting the VBCI model to the specific situation of cyanide bridged species, which requires a number of approximations, we are able to calculate J values with a remarkable accuracy. With the family of Prussian Blue analogs we calculate critical temperatures for both ferro- and ferrimagnetic order. The highest ordering temperatures in Prussian Blue analogs are expected for ferrimagnetic ordering. According to our calculations ordering temperatures much higher than those already achieved should not be expected for Prussian Blue analogs containing 3d metals.

Acknowledgements

We thank J. Bendix, (Caltech, California) for useful comments on the manuscript.

References

[1] Ferlay, S.; Mallah, T.; Ouahés, R.; Veillet, P.; Verdaguer, M. *Inorg. Chem.* **1999**, *38*, 229.
[2] Holmes, S. M.; Girolami, G. S. *J. Am. Chem. Soc.* **1999**, *121*, 5593.
[3] Gadet, V.; Mallah, T.; Castro, I.; Verdaguer, M. *J. Am. Chem. Soc.* **1992**, *114*, 9213.
[4] Mallah, T.; Thiébaut, S.; Verdaguer, M.; Veillet, P. *Science* **1993**, *262*, 1554.
[5] Entley, W. E., Girolami, G. S. *Science* **1995**, *268*, 397.
[6] Babel, D. *Comments Inorg. Chem.* **1986**, *5*, 285.
[7] Klenze, R.; Kanellakopulos, B.; Trageser, G.; Eysel, H. H. *J. Chem. Phys.* **1980**, *72*, 5819.
[8] Gadet, V.; Bujoli-Doeff, M.; Force, L.; Verdaguer, M.; Malkhi, K. E.; Deroy, A.; Besse, J. P.; Chappert, C.; Veillet, P.; Renard, J. P.; Beauvillain, P in *Molecular Magnetic Materials*, Ed. by D. Gatteschi, O. Kahn, J. S. Miller and F. Palacio. Kluwer Academic Publishers 1991, Series E, Vol. 198, p281.

[9] Dujardin, E.; Ferlay, S.; Phan, X.; Desplanches, C.; Cartier dit Moulin, C.; Sainctavit, P.; Baudelet, F.; Dartyge, E.; Veillet, P.; Verdaguer, M. *J. Am. Chem. Soc.* **1998**, *120*, 11347.

[10] Ferlay, S.; Mallah, T.; Ouahés, R.; Veillet, P.; Verdaguer, M. *Nature* **1995**, *378*, 701.

[11] Bozorth, R. M.; Williams, H. J.; Walsh, D. E. *Phys. Rev.* **1956**, *103*, 572.

[12] Griebler, W.-D.; Babel, D. Z. *Naturforsch.* **1982**, *37b*, 832.

[13] Ludi, A.; Güdel H.U. *Structure and Bonding* **1973**, *14*, 1.

[14] Güdel, H. U.; Ludi, A. *Inorg. Chim. Acta* **1972**, *7*, 121.

[15] Anderson, P.W. *Phys. Rev.* **1959**, *115*, 2.

[16] Kahn, O. *Nature* **1995**, *378*, 667.

[17] Scuiller, A.; Mallah, T.; Verdaguer, M.; Nivorozhin, A.; Tholence, J.-L.; Veillet, P. *New J. Chem.* **1996**, *20*, 1.

[18] Mallah, T.; Auberger, C.; Verdaguer, M.; Veillet, P. *J. Chem. Soc., Chem. Commun.* **1995**, 61.

[19] Glerup, J.; Weihe, H. *Acta Chem. Scand.* **1991**, *45*, 444.

[20] Hodgson, D. J.; Michelsen, K.; Pedersen, E.; Towle, D. K.; *Inorg. Chem.* **1991**, *30*, 815–822.

[21] Corbin, K. M.; Glerup, J.; Hodgson, D. J.; Lynn, M. H.; Michelsen, K.; Nielsen, K. M. *Inorg. Chem.* **1993**, *32*, 18.

[22] Zaanen, J.; Sawatzky, G. A.; *Can. J. Phys.* **1987**, *65*, 1262. Didziulis, S. V.; Cohen, S. L.; Gewirth, A. A.; Solomon, E. I. *J. Am. Chem. Soc.* **1988**, *110*, 250. Tuczek, F.; Solomon, E.I. *Inorg. Chem.* **1993**, *32*, 2850. Brown, C. A.; Remar, G. J.; Musselmann, R. L.; Solomon, E. I. *Inorg. Chem.* **1995**, *34*, 688.

[23] Weihe, H.; Güdel, H. U. (*Inorg. Chem.*, accepted).

[24] Wolfsberg, M.; Helmholtz, L.*J. Chem. Phys.* **1955**, *23*, 1841. See also Ballhausen, C. J.; Gray, H. B. *Inorg. Chem.* **1962**, *1*, 111.

[25] Dalgarno, A. in: *Quantum Theory*, Bates, R.D. ed.; Vol. I, 171; Academic Press, New York, 1961.

[26] Lever, A. P. B. *Inorganic Electronic Spectroscopy*, 2. ed. Elsevier 1984.

[27] Riccieri, P.; Zinato, E. *Inorg. Chem.* **1980**, *19*, 853.

[28] Vanquickenborne, L.; Haspeslagh, L.; Hendrickx, M.; Verhulst, J. *Inorg. Chem.* **1984**, *23*, 1677.

[29] Goodenough, J. B. *Magnetism and the Chemical Bond*; Interscience: New York, 1963.

[30] Weihe, H.; Güdel, H. U. *Inorg. Chem.* **1997**, *36*, 3632.

[31] Weihe, H.; Güdel, H. U. *J. Am. Chem. Soc.* **1998**, *120*, 2870.

[32] The quality of these assumptions decrease with increasing n_B, see eqn(13). (See also the discussion of the parameters in section 3 and refs [23, 30, 31]). Hence eqs(10) and (12) under estimate the contributions to J for high n_B.

[33] Nishino, M.; Yoshioka, Y.; Yamaguchi, K. *Chem. Phys. Lett.* **1998**, *297*, 51.

A a AND b BOTH HALF-FILLED

This appendix contains the CI matrices for the particular system illustrated in Figure 1, section 2.1. The triplet matrix has the following form

	1	3	5	9	11
1	0	$-V_B$	V_A	$-V_A^*$	V_B^*
3	$-V_B$	Δ_B	0	0	0
5	V_A	0	Δ_A	0	0
9	$-V_A^*$	0	0	Δ_A^*	0
11	V_B^*	0	0	0	Δ_B^*

(23)

The singlet matrix has the following form

	2	4	6	7	8	10	12
2	0	$-V_B$	$-V_A$	0	0	V_A^*	V_B^*
4	$-V_B$	Δ_B	0	$\sqrt{2}V_A$	0	0	0
6	$-V_A$	0	Δ_A	0	$\sqrt{2}V_B$	0	0
7	0	$\sqrt{2}V_A$	0	U_{AB}	0	$\sqrt{2}V_B^*$	0
8	0	0	$\sqrt{2}V_B$	0	U_{BA}	0	$\sqrt{2}V_A^*$
10	V_A^*	0	0	$\sqrt{2}V_B^*$	0	Δ_A^*	0
12	V_B^*	0	0	0	$\sqrt{2}V_A^*$	0	Δ_B^*

(24)

To fourth order in perturbation theory, the energy difference E(1)-E(0) between the lowest triplet and singlet is given as

$$\begin{aligned} E(1)-E(0) = \quad & V_A^2V_B^2\left[\frac{2}{\Delta_B^2U_{AB}}+\frac{2}{\Delta_A^2U_{BA}}\right] \\ & + V_A^{*2}V_B^{*2}\left[\frac{2}{\Delta_B^{*2}U_{BA}}+\frac{2}{\Delta_A^{*2}U_{AB}}\right] \\ & - V_AV_BV_A^*V_B^*\left[\frac{4}{U_{AB}\Delta_B\Delta_A^*}+\frac{4}{U_{BA}\Delta_A\Delta_B^*}\right] \end{aligned} \quad (25)$$

B *a* HALF-FILLED AND *b* EMPTY

This appendix contains the CI matrices for the particular system illustrated in Figure 2, section 2.2. The triplet matrix has the following form

	1	4	5	7	9	11
1	0	$\sqrt{\frac{4}{3}}V_b$	$-\sqrt{\frac{1}{6}}V_b$	$\sqrt{\frac{1}{2}}V_b$	0	$-V_a^*$
4	$\sqrt{\frac{4}{3}}V_b$	Δ_B	0	0	$\sqrt{\frac{4}{3}}V_a$	0
5	$-\sqrt{\frac{1}{6}}V_b$	0	Δ_B	0	$\sqrt{\frac{2}{3}}V_a$	0
7	$\sqrt{\frac{1}{2}}V_b$	0	0	$\Delta_B+\mathcal{I}_2$	0	0
9	0	$\sqrt{\frac{4}{3}}V_a$	$\sqrt{\frac{2}{3}}V_a$	0	U_{AB}	V_b^*
11	$-V_a^*$	0	0	0	V_b^*	Δ_A^*

(26)

The singlet matrix has the following form

	2	6	8	10	12
2	0	$\sqrt{\frac{3}{2}}V_b$	$\sqrt{\frac{1}{2}}V_b$	0	V_a^*
6	$\sqrt{\frac{3}{2}}V_b$	Δ_B	0	0	0
8	$\sqrt{\frac{1}{2}}V_b$	0	$\Delta_B+\mathcal{I}_2$	$\sqrt{2}V_a$	0
10	0	0	$\sqrt{2}V_a$	$U_{AB}+\mathcal{I}_2$	$-V_b^*$
12	V_a^*	0	0	$-V_b^*$	Δ_A^*

(27)

To fourth order in perturbation theory, the energy difference E(1)-E(0) between the lowest triplet and singlet is given as

$$E(1)-E(0) = -\Bigg\{ V_a^2V_b^2\left[\frac{1}{\Delta_B^2U_{AB}} - \frac{1}{(\Delta_B+\mathcal{I}_2)^2(U_{AB}+\mathcal{I}_2)}\right] + V_a^{*2}V_b^{*2}\left[\frac{1}{\Delta_A^{*2}U_{AB}} - \frac{1}{\Delta_A^{*2}(U_{AB}+\mathcal{I}_2)}\right] - V_aV_bV_a^*V_b^*\left[\frac{2}{\Delta_A^*\Delta_BU_{AB}} - \frac{2}{\Delta_A^*(\Delta_B+\mathcal{I}_2)(U_{AB}+\mathcal{I}_2)}\right] \Bigg\} \quad (28)$$

C *a* HALF-FILLED AND *b* FULL

This appendix contains the CI matrices for the particular system illustrated in Figure 2, section 2.3. The triplet matrix has the following form

	1	3	5	8	9	11
1	0	V_a	0	$-\sqrt{\frac{4}{3}}V_b^*$	$\sqrt{\frac{1}{6}}V_b^*$	$-\sqrt{\frac{1}{2}}V_b^*$
3	V_a	Δ_A	V_b	0	0	0
5	0	V_b	U_{BA}	$\sqrt{\frac{4}{3}}V_a^*$	$\sqrt{\frac{2}{3}}V_a^*$	0
8	$-\sqrt{\frac{4}{3}}V_b^*$	0	$\sqrt{\frac{4}{3}}V_a^*$	Δ_B^*	0	0
9	$\sqrt{\frac{1}{6}}V_b^*$	0	$\sqrt{\frac{2}{3}}V_a^*$	0	Δ_B^*	0
11	$-\sqrt{\frac{1}{2}}V_b^*$	0	0	0	0	$\Delta_B^*+\mathcal{I}_2$

(29)

The singlet matrix has the following form

	2	4	6	10	12
2	0	$-V_a$	0	$-\sqrt{\frac{3}{2}}V_b^*$	$-\sqrt{\frac{1}{2}}V_b^*$
4	$-V_a$	Δ_A	$-V_b$	0	0
6	0	$-V_b$	$U_{BA}+\mathcal{I}_2$	0	$\sqrt{2}V_a^*$
10	$-\sqrt{\frac{3}{2}}V_b^*$	0	0	Δ_B^*	0
12	$-\sqrt{\frac{1}{2}}V_b^*$	0	$\sqrt{2}V_a^*$	0	$\Delta_B^*+\mathcal{I}_2$

(30)

To fourth order in perturbation theory, the energy difference E(1)-E(0) between the lowest triplet and singlet is given as

$$
\begin{aligned}
E(1)-E(0) = -\Bigg\{ & V_a^2V_b^2\left[\frac{1}{\Delta_A^2U_{BA}}-\frac{1}{\Delta_A^2(U_{BA}+\mathcal{I}_2)}\right] \\
& + V_a^{*2}V_b^{*2}\left[\frac{1}{\Delta_B^{*2}U_{BA}}-\frac{1}{(\Delta_B^{*2}+\mathcal{I}_2)^2(U_{BA}+\mathcal{I}_2)}\right] \\
& - V_aV_bV_a^*V_b^*\left[\frac{2}{\Delta_A\Delta_B^*U_{BA}}-\frac{2}{\Delta_A(\Delta_B^*+\mathcal{I}_2)(U_{BA}+\mathcal{I}_2)}\right]\Bigg\}
\end{aligned}
\tag{31}
$$